AGU PUBLICATIONS

Global Biogeochemical Cycles

RESEARCH ARTICLE
10.1002/2013GB004708

**Key Points:**
- Ocean oxygenation varies inversely with easterly wind stress magnitude
- Changes in ocean ventilation and biological activity are the dominant drivers
- Indian OMZ opposes effect of south Pacific OMZ, which drives the global response

**Correspondence to:**
N. N. Ridder,
n.ridder@unsw.edu.au

**Citation:**
Ridder, N. N., and M. H. England (2014), Sensitivity of ocean oxygenation to variations in tropical zonal wind stress magnitude, *Global Biogeochem. Cycles*, *28*, 909–926, doi:10.1002/2013GB004708.

Received 7 AUG 2013
Accepted 29 JUL 2014
Accepted article online 1 AUG 2014
Published online 3 SEP 2014

# Sensitivity of ocean oxygenation to variations in tropical zonal wind stress magnitude

**Nina N. Ridder[1] and Matthew H. England[1]**

[1] Australian Research Council Centre of Excellence for Climate System Science, University of New South Wales, Sydney, New South Wales, Australia

**Abstract** Ocean oxygenation has been observed to have changed over the past few decades and is projected to change further under global climate change due to an interplay of several mechanisms. In this study we isolate the effect of modified tropical surface wind stress conditions on the evolution of ocean oxygenation in a numerical climate model. We find that ocean oxygenation varies inversely with low-latitude surface wind stress. Approximately one third of this response is driven by sea surface temperature anomalies; the remaining two thirds result from changes in ocean circulation and marine biology. Global mean $O_2$ concentration changes reach maximum values of +4 μM and −3.6 μM in the two most extreme perturbation cases of −30% and +30% wind change, respectively. Localized changes lie between +92 μM under 30% reduced winds and −56 μM for 30% increased winds. Overall, we find that the extent of the global low-oxygen volume varies with the same sign as the wind perturbation; namely, weaker winds reduce the low-oxygen volume on the global scale and vice versa for increased trade winds. We identify two regions, one in the Pacific Ocean off Chile and the other in the Indian Ocean off Somalia, that are of particular importance for the evolution of oxygen minimum zones in the global ocean.

## 1. Introduction

Marine life and biogeochemical processes are highly dependent on the oxygen ($O_2$) content of the ocean. Concentrations of $O_2$ below certain thresholds can disturb whole ecosystems and have a high impact on the cycling of important oceanic tracers, such as carbon and nitrogen. Three different concentration limits are of particular interest when studying the effect of dissolved $O_2$ on marine biogeochemistry: (i) hypoxia, (ii) suboxia, and (iii) anoxia. Hypoxic conditions are those under which certain species suffer from an insufficient amount of $O_2$ for respiration, thus making these regions uninhabitable for that particular species. The minimum $O_2$ concentration which marks the border to hypoxic conditions varies depending on species. For the purpose of this paper we follow the definition of *Gnanadesikan et al.* [2012] who define the threshold for hypoxia to be at 88 μM. In suboxic waters nitrogen is involved in remineralization (denitrification) instead of $O_2$, reducing the availability of nitrogen as a nutrient for other biogeochemical processes, i.e., photosynthesis [e.g., *Codispoti et al.*, 2001; *Oschlies et al.*, 2008]. Most species are unable to survive under suboxic conditions [*Oschlies et al.*, 2008]; hence, regions with these low-oxygen concentrations are often referred to as "Dead Zones" or Oxygen Minimum Zones (OMZs) [*Cline and Richards*, 1972]. We again follow *Gnanadesikan et al.* [2012] and refer to water masses with $O_2$ concentrations below 8.8 μM as suboxic. Anoxic conditions describe waters that contain $O_2$ concentrations below 0.1 μM [*Oguz et al.*, 2000]. At this threshold, sulfate reduction occurs and starts to replace $NO_3$ respiration [*Paulmier and Ruiz-Pino*, 2009].

Low-oxygen conditions can be found in eastern boundary shadow zones and are caused by a combination of high biologic activity [e.g., *Helly and Levin*, 2004] and minimal lateral renewal of surface waters [*Reid*, 1965]. The strongest OMZs are located in the Pacific Ocean and contain $O_2$ concentrations below 0.1 μM. The Atlantic and Indian Oceans contain similar low-oxygen zones but do not reach anoxic conditions [*Paulmier and Ruiz-Pino*, 2009; *Stramma et al.*, 2010]. A change in the oxygenation of the ocean, and with this in the volume of low-oxygen waters, will potentially significantly affect the carbon and nitrogen cycles as well as the removal of other greenhouse gases from the atmosphere. This can lead to an amplifying feedback on global climate change as reduced biological productivity implies reduced ocean carbon uptake. Observations show a negative trend in the ocean oxygenation and suggest that low-oxygen regions have been expanding in volume over the past few decades [e.g., *Stramma et al.*, 2008, 2010, 2012].

Model studies have so far yielded contradicting results regarding the future fate of low-oxygen regions under global climate change. Several studies suggest an expansion of suboxic conditions [e.g., *Shaffer et al.*, 2009; *Frölicher et al.*, 2009] due to an increase in stratification causing a reduction in ocean ventilation [*Matear et al.*, 2000; *Bopp et al.*, 2002]. Other studies contradict these projections; for example, *Duteil and Oschlies* [2011] show that the choice of the background diapycnal mixing can dampen the effect of global climate change on OMZs. *Matear and Hirst* [2003] find that due to a reduction in export production in the low-oxygen regions, $O_2$ concentrations in the tropical thermocline can increase in global warming simulations. *Gnanadesikan et al.* [2012] also find increased $O_2$ concentrations in one of the strongest OMZs in the southeast Pacific off Chile. In their study a shift in surface winds to a more along-shore orientation of wind stress due to changes in atmospheric circulation, in particular the strengthening of the subtropical high over this region, leads to higher oxygenation of waters off Chile at the core of the OMZ. This result is of particular interest as the Walker circulation and with this equatorial winds have been observed to have changed over the past few decades [e.g., *Harrison*, 1989; *Trenberth and Hurrell*, 1994; *Clarke and Lebedev*, 1996; *Vecchi and Soden*, 2007; *L'Heureux et al.*, 2013]. Several model and observational studies further suggest that low-latitude winds are likely to change further under global warming due to changes in the strength of the atmospheric equatorial zonal circulation [e.g., *Vecchi et al.*, 2006; *Vecchi and Soden*, 2007; *Collins et al.*, 2010; *Tokinaga and Xie*, 2011; *Tokinaga et al.*, 2012]. However, as yet there is no consensus on whether this circulation will strengthen or weaken. A change in zonal atmospheric circulation at low latitudes would likely affect the future evolution of low-oxygen zones in significant ways, for example, via potential changes in circulation, upwelling, interior advection of oxygen, and nutrient fluxes, which have been shown to induce changes in ocean biogeochemistry [*Ridder et al.*, 2013]. To elaborate the sensitivity of ocean oxygenation to low latitude surface winds, we assess the impact of different tropical zonal easterly surface wind stress fields (hereafter $\tau_x$) on global mean $O_2$ concentrations as well as on low-oxygen regions using a coupled climate model of intermediate complexity.

## 2. Model and Experimental Setup

This study uses the University of Victoria Earth System Climate Model (UVic ESCM v2.9), which consists of a full ocean global circulation model (OGCM) based on the Geophysical Fluid Dynamics Laboratory Modular Ocean Model in Version 2.2 [*Pacanowski*, 1995] coupled to a two-dimensional energy-moisture balance model of the atmosphere, a thermodynamic/dynamic sea ice model [*Semtner*, 1976; *Hibler*, 1979; *Hunke and Dukowicz*, 1997], a land surface scheme, a vegetation model (Top-down Representation of Interactive Foliage and Flora Including Dynamics (TRIFFID)) [*Meissner et al.*, 2003], and a sediment model [*Archer*, 1996]. The OGCM has a zonal resolution of 3.6° and a meridional resolution of 1.8° with 19 vertical levels. Ocean circulation is forced by a monthly cycle wind climatology which for this study is predescribed by reanalysis winds from the National Center for Environmental Prediction (NCEP) [*Kalnay et al.*, 1996].

An nutrient-phytoplankton-zooplankton-detritus model, which is nested within the OGCM, accounts for processes related to marine biology [*Schmittner et al.*, 2008]. Organic parameters are incorporated in the form of zooplankton and detritus and different classes of phytoplankton, nitrogen fixing diazotrophs, and other phytoplankton. Oxygen concentrations are determined using a constant stoichiometry in relation to availability of nutrients, namely, $NO_3$ and $PO_4$. The source term of oxygen includes the air-sea flux of $O_2$ and is inversely proportional to the sink term of $PO_4$ and therefore phytoplankton growth. The model thus represents photosynthesis as a reduction in $PO_4$ in combination with a production of $O_2$ at the same rate. Conversely, respiration consumes oxygen; in the model this occurs at a rate equal to the remineralization of $PO_4$. The marine biological model accounts for a decrease in remineralization rate in low-oxygen environments ($[O_2] < 10$ μM). Following Ocean Carbon-Cycle Model Intercomparison Project recommendations, it limits $O_2$ consumption below concentrations of 5 μmol $kg^{-1}$ and includes denitrification as a nutrient sink in these regions. In its current version the model slightly overestimates the production of oxygen due to (i) nitrogen fixation, as it assumes the same stoichiometry here as for primary production, and (ii) the continuation of remineralization under truly anoxic and nitrate-depleted conditions. However, while this results in an increase in the modeled global mean surface oxygen flux by about 0.05 mol $O_2$ $m^{-2}$ $yr^{-1}$, the effect on relative changes in the air-sea $O_2$ exchange between the different experiments are insignificant. The impact on modeled global mean $O_2$ concentrations, denitrification, remineralization, and the extent of low-oxygen volumes, in general, are also negligible. A detailed description of the marine biological model can be found in *Schmittner et al.* [2008].

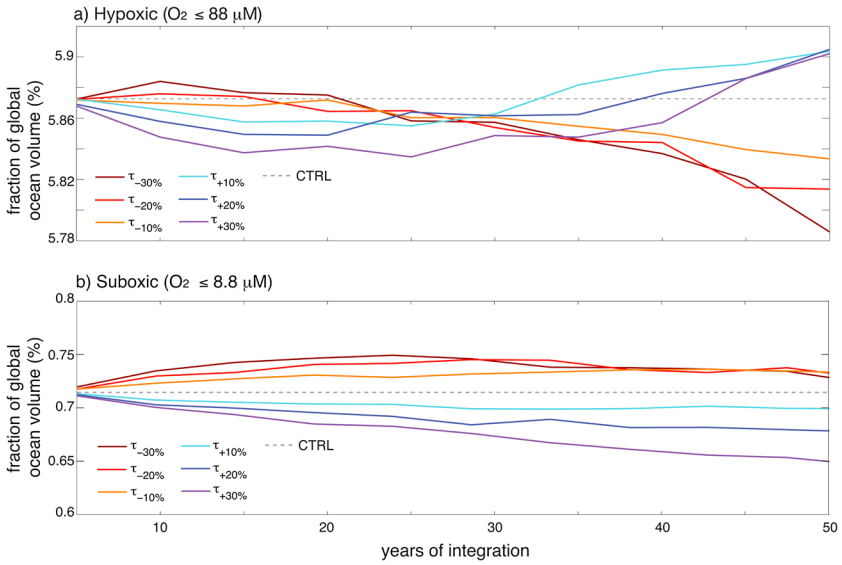


**Figure 1.** Evolution of the fraction of the (a) hypoxic ($[O_2] \in [0.0\ \mu M; 88.0\ \mu M]$) and (b) suboxic ($[O_2] \in [0.0\ \mu M; 8.8\ \mu M]$) water mass volume under transient wind changes. Note the different *y* axis scales in Figure 1a and 1b.

The UVic ESCM has been verified against observational data and proven to be able to represent ocean properties, including ocean circulation, temperature, salinity, and biological processes reasonably well [e.g., *Weaver et al.*, 2001; *Schmittner et al.*, 2008]. Despite a small warm bias in sea surface temperatures (SSTs) of roughly 0.39°C over observed low-oxygen regions, indicating shortcomings in the representation of the Eastern Boundary Upwelling System, the model is able to reproduce the oceanic oxygen inventory within 3% of the value provided by the World Ocean Atlas [*Oschlies et al.*, 2008] and reaches a correlation coefficient of 0.9 [*Cocco et al.*, 2013]. Like most OGCMs, the UVic ESCM overestimates the extent and strength of low-oxygen regions slightly; nevertheless, the model captures their broad observed patterns reasonably well [*Oschlies et al.*, 2008; *Cocco et al.*, 2013]. For further assessment of the performance of the UVic ESCM in regard to key biogeochemical parameters, the reader is referred to *Cocco et al.* [2013].

In this study the UVic ESCM is used to perform seven model experiments to assess the impact of changed low-latitude wind conditions on ocean oxygenation. A similar study has been undertaken exploring identical wind stress anomalies and their impact on dissolved inorganic carbon [*Ridder et al.*, 2013]. Here we assess the same wind stress changes and their impact on dissolved oxygen. The reference scenario (hereafter CTRL) uses monthly average NCEP reanalysis wind fields. The six additional experiments use NCEP data with changed conditions in the latitudes between 30°N and 30°S. These changes consist of decreases in the easterly zonal wind stress component by factors of 10%, 20%, and 30% (hereafter $\tau_{-10\%}$, $\tau_{-20\%}$, and $\tau_{-30\%}$, respectively) and equivalent increases in the easterly components (hereafter $\tau_{+10\%}$, $\tau_{+20\%}$, and $\tau_{+30\%}$). The westerly component of the zonal surface wind stress as well as the wind speed, and with this the gas piston velocity, remains unchanged, both inside the tropics and globally. This idealized approach of systematically changing easterly wind stress is used to simplify the identification of the wind-driven mechanisms determining ocean oxygenation. Under more realistic conditions, any variation in the Walker Circulation is expected to result in more complex wind stress changes, with regionally varying conditions of strengthened or weakened winds. This should be kept in mind when interpreting the results of this study, which aims to assess the sensitivity of ocean oxygenation to large-scale wind stress changes and the associated ocean dynamics and biogeochemical mechanisms, with implications for predictions of the future evolution of dissolved oxygen.

All model experiments commence from an equilibrated simulation, which used contemporary forcing fields and was integrated for 8000 years. The model experiments then run until an equilibrium under the new wind conditions is reached. Additionally, a set of transient perturbation experiments has been performed, in which the perturbation starts at time $t = 0$ and is ramped up from zero to maximum wind anomalies of ±10%, ±20%, and ±30% over half a century. Observed multidecadal variability in the Pacific zonal wind stress, which has recently been demonstrated to have varied between around ±10 and 20% during the past century, with peaks of over ±30% [*England et al.*, 2014], leaves the chosen perturbation anomalies well

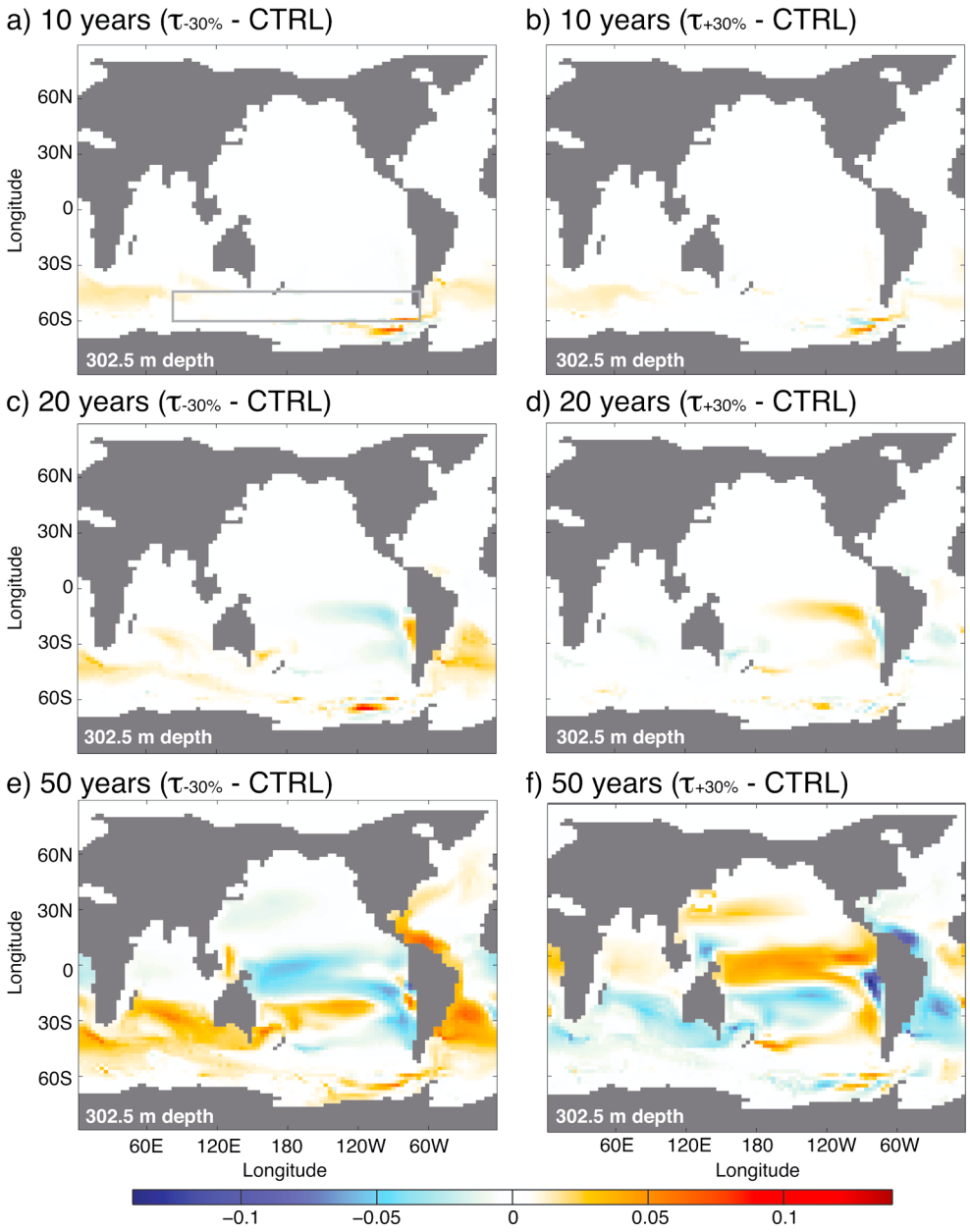


**Figure 2.** Changes in SAMW transport under a transient introduction of wind stress perturbations. Color shading shows the difference in dye tracer (dimensionless) at 302.5 m depth between (a, c, and e) $\tau_{-30\%}$ − CTRL and (b, d, and f) $\tau_{+30\%}$ − CTRL 10 years (Figures 2a and 2b), 20 years (Figures 2c and 2d), and 50 years (Figures 2e and 2f) after the onset of the perturbation. Grey box in Figure 2a marks surface area where dye tracer was released.

within the observed range of variability. Furthermore, future trends in tropical zonal winds and the Walker Circulation could also span this range [see, e.g., *Collins et al.*, 2010]. The atmospheric $CO_2$ concentration was fixed at 369 ppm in all wind field scenarios.

A passive dye tracer is introduced into the OGCM to track changes in Subantarctic Mode Water (SAMW). The dye tracer follows the model's transport equation for tracers such as temperature and salinity but is restored to one at the surface between 58.5°S–45.9°S and 70.2°E–70.2°W at every time step. Everywhere else, the dye tracer is initiated with a concentration of zero and it then evolves freely according to the modeled ocean transport. To additionally allow the determination of ventilation time changes due to the applied wind stress perturbations, a second tracer, a passive age tracer, has also been implemented in the model

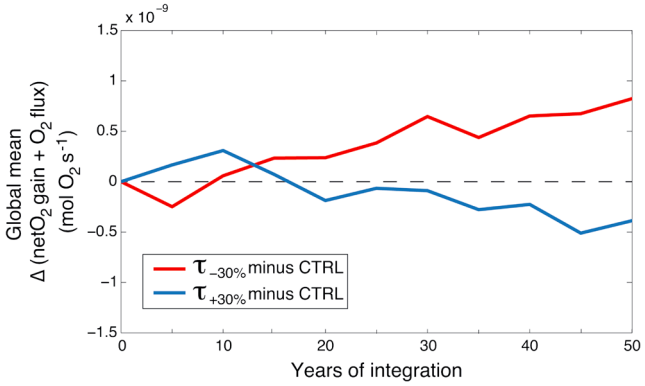


**Figure 3.** Evolution of global mean net $O_2$ gain (through denitrification and nitrogen fixation) and oxygen release to the atmosphere under transient wind stress changes compared to CTRL. For clarity, only the response to the transient introduction of 30% stronger (minus CTRL, blue) and weaker (minus CTRL, red) winds are shown.

(as per *England* [1995]). This age tracer also follows the model's transport equation for tracers and is also set to zero everywhere at the beginning of the model integration. However, the age tracer is then increased everywhere and at every time step by a constant value equal to the length of the ocean model time step, except in the surface layer, where the tracer is set to retain a constant value of zero throughout the run. To facilitate an accurate analysis of water mass age changes, the age tracer was introduced into the equilibrated experiments under the chosen wind stress field and was integrated until the age tracer reaches an equilibrium with age changes of less than 6 months per century of integration (as in *England* [1995]). The age changes yielded by this new tracer are in broad agreement with the age changes derived from radiocarbon concentration ($\Delta^{14}C$ anomaly) changes (not shown).

## 3. Transient Experiments

### 3.1. Changes in the OMZs

In the first decades after the onset of a transient introduction of the wind stress perturbations, the hypoxic and suboxic volumes, both respond with the opposite sign compared to the applied perturbation, i.e., low-oxygen volumes expand for weakening winds and contract for strengthening winds (Figure 1). This behavior is caused by the wind-induced changes in the supply of oxygen-rich subsurface waters from the equatorial western to the eastern boundary of each basin, which is one of the major sources of the ventilation for low-oxygen regions, particularly in the equatorial Pacific [*Stramma et al.*, 2008]. The easterward equatorial subsurface transport (at 170°W, between 15°S–15°N and 50 m–600 m depth) within the Pacific Ocean for instance decreases almost linearly from 16.5 sverdrup (Sv) in CTRL to 9.1 Sv in equilibrium following the decline in wind stress of up to 30%, while increased winds lead to stronger eastward subsurface currents (23.6 Sv in experiment $\tau_{+30\%}$ in equilibrium).

The evolution of the hypoxic volume experiences a change in sign after approximately 20 to 30 years of transient wind stress change. The suboxic volume experiences a similar sign reversal later in the model integration (not shown). In both cases the reversal of sign is caused by a combination of changes in (i) the atmosphere-ocean $O_2$ flux due to modified dissolved oxygen concentrations, (ii) denitrification as a result of the variations in the suboxic volume, and (iii) nitrogen fixation caused by changes in the number of diazotrophs due to altered nutrient upwelling. In the case of weakening trade wind conditions the expansion of the suboxic volume forces an increase in anaerobic remineralization, which acts as a source of $O_2$. The simultaneous reduction in nitrogen fixation, which removes $O_2$ to form $NO_3$, and in the outgassing of $O_2$ due to initially lower oxygen concentrations, then lead to a net gain in $O_2$. In combination with increases in the ventilation of the South Pacific shadow zone and the supply of oxygen-rich waters from high latitudes, which can be seen in the increase in SAMW formation off Peru/Chile (Figure 2, discussed in detail below), the modifications in the nitrogen cycle eventually reverse the sign of change in the global hypoxic volume (Figure 3). The same mechanisms but of opposite sign are at play under strengthening wind conditions.

### 3.2. Global Oxygen Changes

A transient introduction of the wind perturbations ramped up over 50 years initially shows global mean oxygen concentration changes of the same sign as the perturbation, i.e., decreasing global mean $O_2$ for weakened winds and vice versa for strengthened winds following the evolution of the oceanic low-oxygen volume as described above (Figures 4a and 4b). The maximum signature of change in this early phase of the wind perturbations is reached between 10 and 15 years into the integration and scales approximately with the perturbation. After around 20 years of integration the net global ocean oxygenation begins to reverse

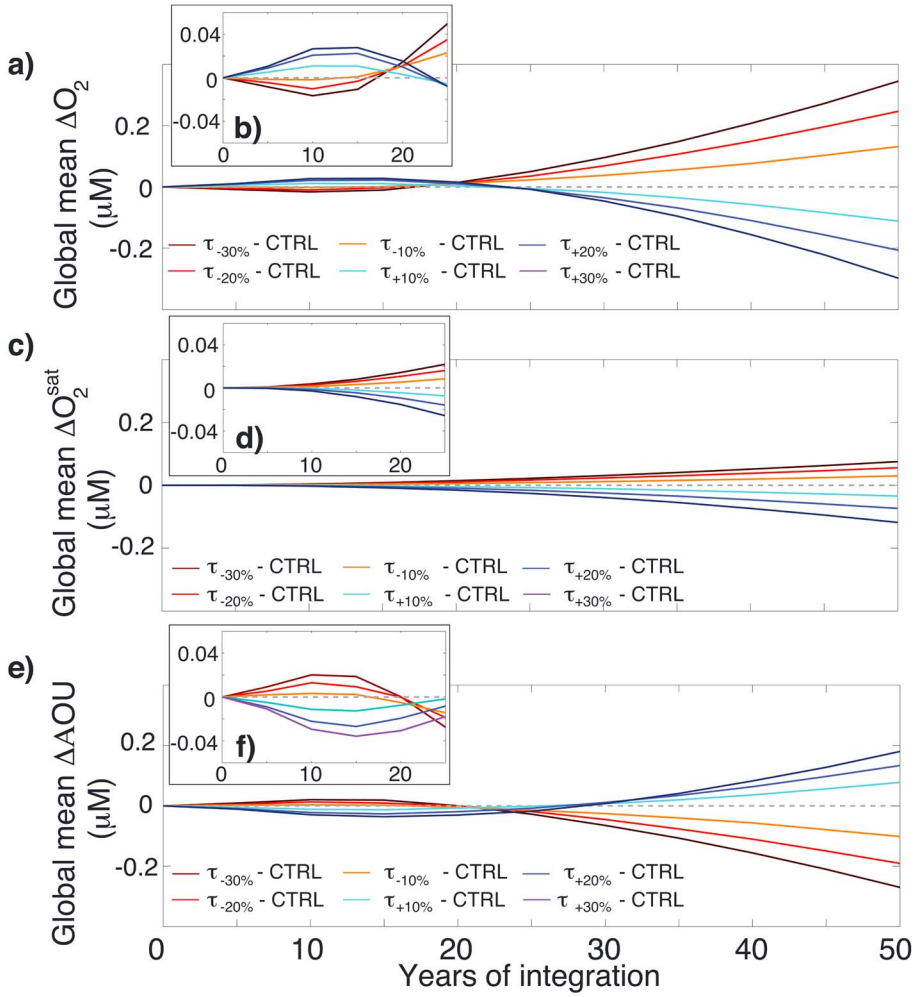


**Figure 4.** Evolution of global mean (a, b) oxygen concentration, (c, d) oxygen saturation concentration ($O_2^{sat}$), and (e, f) apparent oxygen utilization (AOU) all in μM under transient implementation of low-latitude wind perturbations.

in its tendency, with decreasing concentrations for increasing winds, and vice versa for reduced magnitude winds. Thereafter, oxygen changes are almost linear in time in all experiments (Figure 4a).

One third of the changes in global mean $O_2$ can be accounted for by the transient response of the oxygen saturation concentration ($O_2^{sat}$) [*Weiss*, 1970] (Figures 4c and 4d). These are caused by temperature changes and are of the opposite sign compared to the wind perturbation throughout the whole integration, i.e., negative for strengthened winds and vice versa for weakened winds.

The response of apparent oxygen utilization (AOU, Figures 4e and 4f) dominates the response of global mean $O_2$ in all experiments and is the reason for the change of sign in the response of global mean $O_2$ within the first two decades after the introduction of the wind perturbations. The transient changes in AOU in the first decades after the onset of the perturbation are driven by the initial response of the OMZs to modifications in the lateral ventilation of eastern boundary shadow zones and the resulting changes in the nitrogen cycle affecting oxygen consumption, as discussed above. The sign reversal is caused by a combination of the changes in (i) atmosphere-ocean $O_2$ flux due to varied dissolved oxygen concentrations, (ii) denitrification as a result of the volume changes of the suboxic regions, and (iii) nitrogen fixation caused by a variation in the number of nitrogen fixing diazotrophs due to the changed rate of upwelling of nutrients (see above).

Changes in ocean transport from the southern to low latitudes start to contribute to the response of global mean $O_2$ concentrations to wind perturbations about 20 years after the onset of the transient perturbation. At this time water that had been ventilated at high latitudes during the onset of the perturbation is now returning nutrients and oxygen-rich waters (via SAMW; *Sarmiento et al.*, 2004; *Rodgers et al.*, 2003) to the

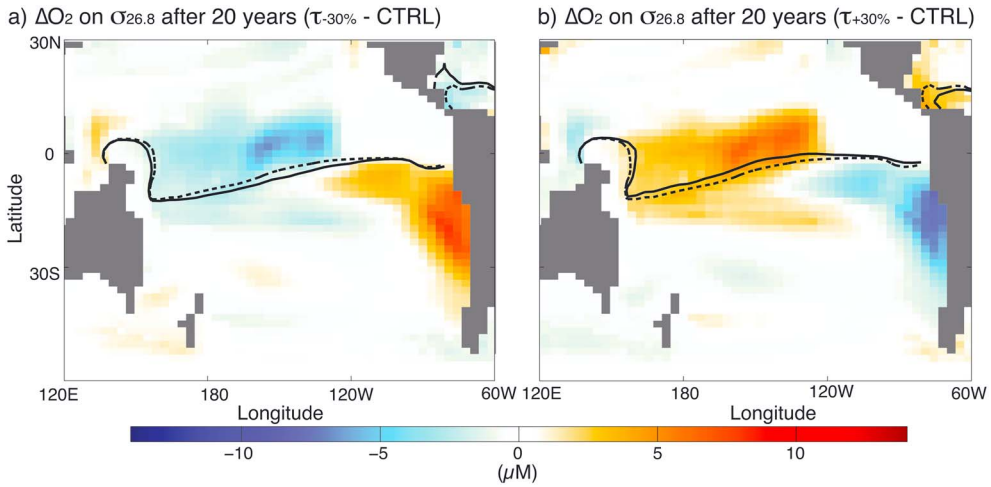


**Figure 5.** (a) Pacific oxygen concentration change (μM) in SAMW (here taken to be on the $\sigma_{26.8}$ isopycnal) 20 years after the onset of a transient wind perturbation, $\tau_{-30\%}$ − CTRL. Contour lines indicate the extent of SAMW dye with [dye]<0.001 north of contours and [dye]>0.001 south of contours, solid line represents dye in $\tau_{-30\%}$, and dotted line shows dye in CTRL. (b) As Figure 5a but for $\tau_{+30\%}$ − CTRL and $\tau_{+30\%}$ for solid contour lines.

equatorial region (Figure 2b). At the same time the wind-driven slow down of the South Pacific subtropical gyre leads to a more ventilated South Pacific shadow zone, with more SAMW entering the Pacific OMZ, thus increasing $O_2$ concentrations in this region and offsetting the reduction in biological $O_2$ production at low latitudes (Figure 2). An increased $O_2$ concentration in SAMW due to the reduction in the global mean remineralization of organic material amplifies this oxygenating effect in the South Pacific Ocean despite a moderate weakening of the SAMW transport reaching the equatorial region (Figure 5). This change in $O_2$ transport compensates for the reduced inflow of oxygen-rich waters into the equatorial southeast Pacific and, together with the changes in marine biology, finally reverses the change in global ocean oxygenation over time (Figures 4a and 4b). The same mechanisms but of opposite sign are at play under strengthened wind stress conditions. Here an initial increase in the inflow of oxygen to the eastern boundary low-oxygen volumes in the first decades of the perturbation is replaced by an overall decrease in global mean $O_2$ due to (i) an increased loss of oxygen to the atmosphere and in the nitrogen cycle, (ii) an expansion of the South Pacific shadow zone, and (iii) decreased $O_2$ concentrations in SAMW compared to normal wind conditions.

## 4. Equilibrium Response

### 4.1. Changes in OMZs

In equilibrium the volumes of water masses within the global ocean with hypoxic and suboxic conditions expand under increased tropical easterly wind stress and contract under decreased winds (Figure 6), generally continuing the trend of the transient experiments. The global equilibrium response of the low-oxygen volumes is dominated by the Pacific Ocean, which exhibits a high sensitivity to the applied perturbations (Figure 6). The Indian Ocean shows changes of the opposite sign compared to the Pacific and the Atlantic Ocean. Both the Pacific and the Indian Oceans exhibit a pattern of increased $O_2$ in the east and decreased $O_2$ in the west of the basin for weaker wind stress and vice versa for stronger winds (Figures 7a, 7b, 8a, and 8c). In the Pacific Ocean the eastern boundary off Chile (at 32°S–8°S, 272°E–290°E and at 240–550 m depth; Figures 7c, 7d, 8a, and 8c) develops changes of higher amplitude compared to the changes at the western boundary. In fact, the changes in $O_2$ at the eastern boundary dominate the response of the whole Pacific basin and reduce the extent of the Pacific OMZ.

The Indian Ocean reacts in the opposite sense, with higher changes at the western boundary off Somalia and Kenya (at 9°S–9°S, 42°E–82°E and at 240–500 m depth; Figures 7a, 7b, 8a, and 8c) determining the overall response of the Indian Ocean low-oxygen volume. This leads to contracting low-oxygen volumes in the Pacific basin and expanding low-oxygen water masses in the Indian Ocean for weakened surface wind stress (vice versa for strengthened winds). The difference between the two ocean basins is caused by their different geometry: the Pacific Ocean has an enclosed eastern boundary with a strong upwelling region, which sets the response in $O_2$ via changes in the nutrient supply from greater depths and hence local

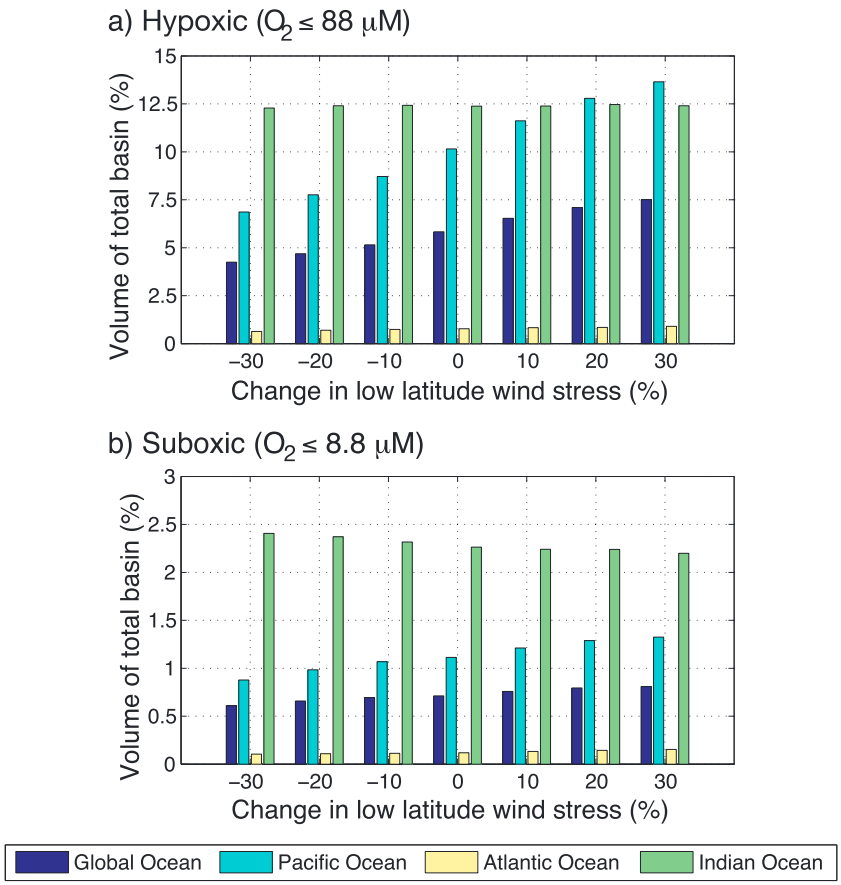


**Figure 6.** Fraction of the (a) hypoxic ($[O_2] \in [0.0\ \mu M; 88.0\ \mu M]$) and (b) suboxic ($[O_2] \in [0.0\ \mu M; 8.8\ \mu M]$) water mass volume in the global (navy), Pacific Ocean (blue), Atlantic Ocean (yellow), and the Indian Ocean (green) in equilibrium with the perturbed low-latitude surface wind stress conditions (%). Note the different *y* axis scales in Figures 6a and 6b.

biological activity and remineralization in addition to the meridional inflow of oxygen-rich waters. The eastern boundary of the Indian Ocean, in contrast, is influenced not only by local upwelling and meridional supply of dissolved oxygen but also by the supply of oxygen-rich waters from the Pacific Ocean via variations in the Indonesian throughflow, which weakens for a decline in surface wind stress and vice versa for strengthened winds. The Indonesian throughflow partially compensates the upwelling fluxes along the eastern boundary of the Indian Ocean so that the western boundary region exhibits the strongest net response to wind variations within the Indian basin.

In the low-oxygen waters off Chile the decreased $\tau_x$ experiments cause an increased meridional and vertical supply of oxygen to the low-oxygen region (Figures 9c and 9d). One of the major mechanisms behind this change is a decrease in the strength of the Equatorial Undercurrent (EUC) System and the South Equatorial Current (SEC) (Figure 8b), which in combination with a stronger proportional component in the along-shore winds results in an increased inflow of oxygen-rich waters from the south where colder temperatures facilitate increased oxygen concentrations (Figures 10e and 9c). Additionally, the region experiences an increase in net upwelling (Figure 9d), which supplies more oxygen from greater depths, where decreased remineralization (Figure 11) leads to higher $O_2$ concentrations. This decrease in remineralization, and with this the reduction in oxygen depletion, results from a decreased import of organic material from shallower layers above 240 m, where reduced upwelling results in lower biological activity and thus export production (Figure 9). The changes in net upwelling are caused by a slower Ekman transport away from the equator. This reduces the downwelling of water in the descending branch of the equatorial overturning cells, which completely compensates for the reduced upwelling at the eastern boundary of the basin. Experiment $\tau_{+30\%}$ shows similar results but of the opposite sign (Figures 9e and 9f). Experiments incorporating smaller perturbations exhibit similar patterns of response and mechanisms, although of reduced amplitude

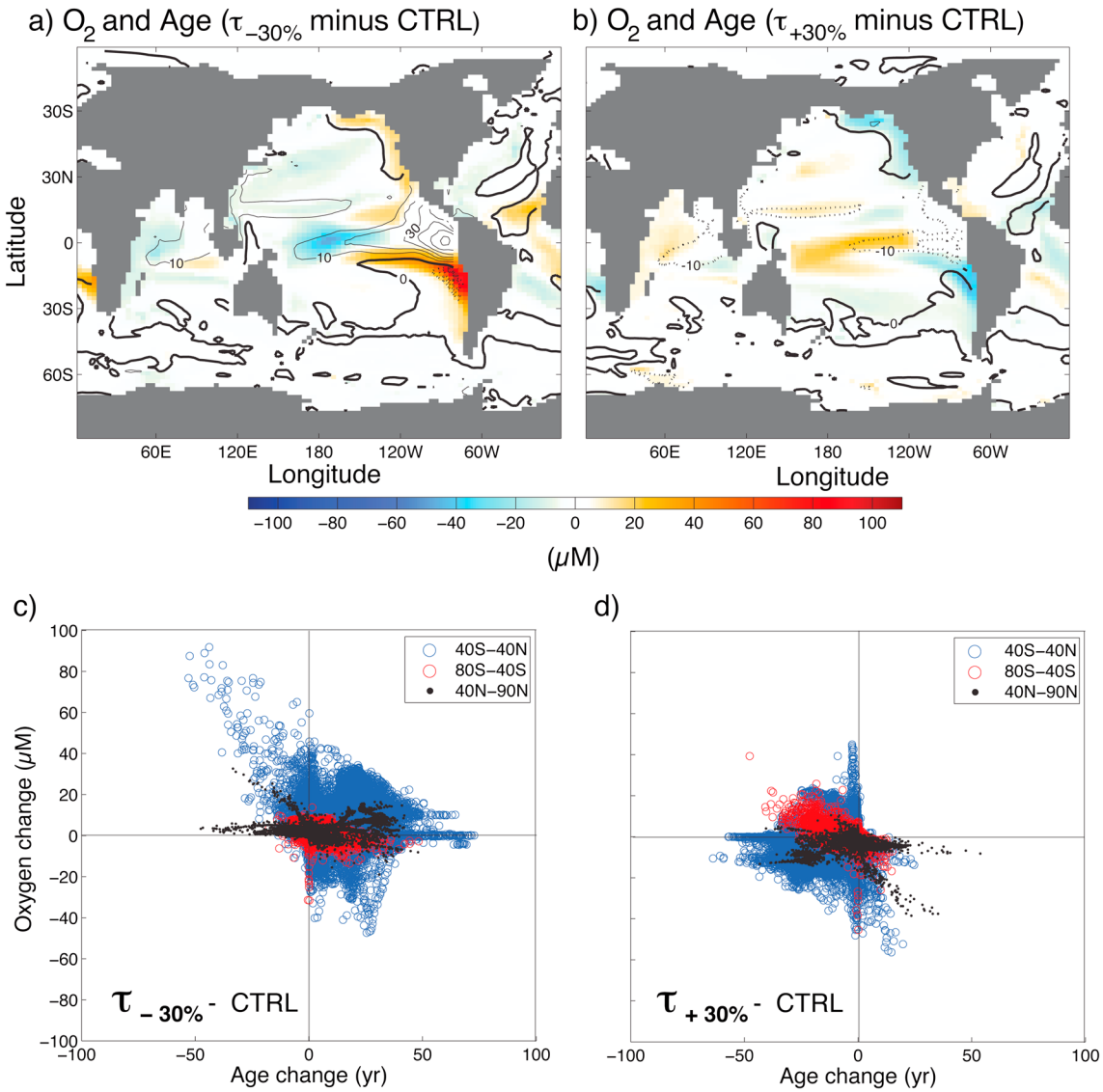


**Figure 7.** (a) Oxygen changes (oxygen saturation effects removed; shading) in μM and age changes (yr; contours) at 302.5 m depth in equilibrium with perturbations in experiment $\tau_{-30\%}$ relative to CTRL. The thin solid lines mark regions with older water, dotted lines indicate younger water, and zero contour is solid bold. Contour interval is 10 years. (b) As Figure 7a but for experiment $\tau_{+30\%}$ − CTRL. (c) Scatterplot of $O_2$ changes (μM) and age changes (yr) in different latitude bands in experiment $\tau_{-30\%}$ relative to CTRL. (d) As Figure 7c but for experiment $\tau_{+30\%}$ − CTRL.

(not shown). It may be noted, however, that the relative coarse resolution of the UVic ESCM limits the accuracy in representing near-coast winds, which are essential for the dynamics of the Eastern Boundary Upwelling systems. Therefore, the modeled change in the coastal upwelling regions may be biased by the model's coarse resolution.

The region off Somalia responds with a weakening of the southern subtropical gyre (Figure 8b), which leads to a decreased inflow of water from the south (Figure 12c). This results in a loss of $O_2$ in this region, expanding the OMZ in $\tau_{-30\%}$ compared to CTRL. At the same time, the zonal transport of oxygen-rich waters from the east (north of 10°S) into the OMZ is increased. However, this cannot compensate for the decreased supply of $O_2$ due to the decreased inflow caused by the weakened gyre (Figures 12c and 12d). Also, a decrease in remineralization, which derives from reduced import of organic material from shallower layers above 240 m with lower NPP (Figure 12), cannot fully compensate for the decreased supply of oxygen from the south. Increasing the surface wind stress in the tropics causes a similar pattern of response, but of the opposite sign, leading to an overall increase in $O_2$ in the Indian Ocean OMZ (Figures 12e and 12f).

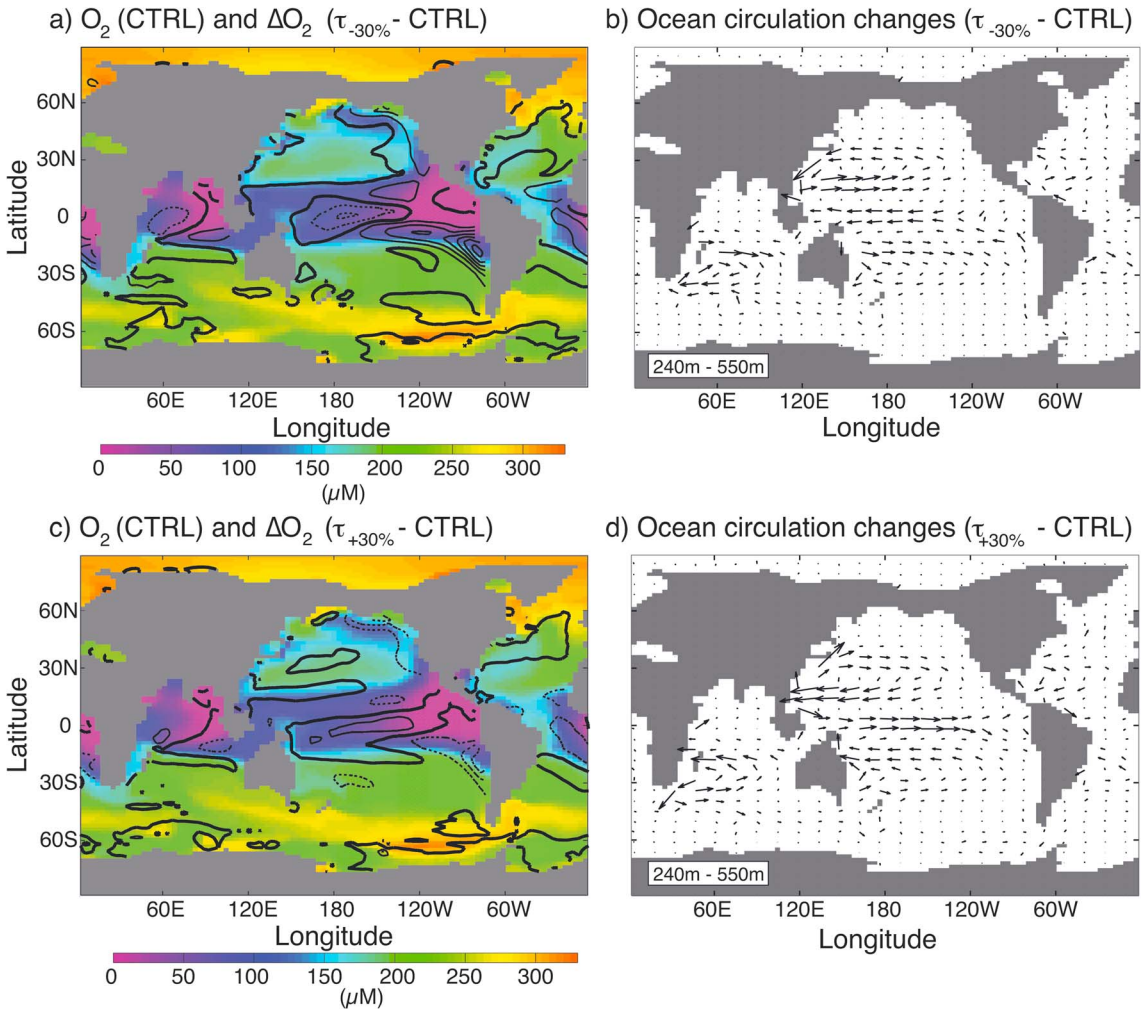


**Figure 8.** (a) Oxygen concentration (μM) averaged over 240 m to 550 m in CTRL (color shading). Contours show the difference in oxygen concentration averaged over the same depth range ($\tau_{-30\%}$ − CTRL). Dashed lines indicate a decrease in equilibrated $O_2$ in $\tau_{-30\%}$ compared to CTRL, and solid lines represent an increase in equilibrated $O_2$ ($\tau_{-30\%}$ − CTRL). The zero contour is solid bold; contour intervals are 10 μM. (b) Changes in ocean circulation averaged over 240 m to 550 m depth ($\tau_{-30\%}$ − CTRL). (c and d) As Figures 8a and 8b, respectively, only for $\tau_{+30\%}$ − CTRL.

### 4.2. Global Oxygen Changes

In equilibrium, the overall response in global mean concentration of $O_2$ is consistent with the transient experiments, leading to a more oxygenated ocean under weakened wind stress and vice versa for increased wind conditions, scaling almost linearly with the magnitude of perturbation (Figure 13a). In agreement with the results described in the transient perturbations, roughly one third of the $O_2$ change can be accounted for by changes in temperature, i.e., oxygen saturation concentrations ($O_2^{sat}$; Figure 13b). This derives from changes in sea surface temperature (SST), which, in case of a $\tau_x$ decrease, show a warm anomaly limited to the equatorial Pacific and Atlantic Ocean stretching westward from the eastern boundary of the basin (Figure 10). The remaining surface ocean at middle- and high-latitudes experience a decrease in SST increasing $O_2^{sat}$ in areas where intermediate and deep waters are formed. The changes in the air-sea $O_2$ flux confirms that SST changes overall lead to a decreased release of $O_2$ from the ocean into the atmosphere under decreased trade wind conditions (Figures 11 and 14). Strengthened wind conditions cause a similar response but of opposite sign. The anomalies scale with the applied wind perturbation, with $\tau_{-30\%}$ and $\tau_{+30\%}$ showing the highest net integrated $O_2$ changes.

Alterations in AOU account for the main part of the response in global mean $O_2$ (compare Figures 13a and 4a to Figures 13c and 4c, respectively). The AOU changes are in turn driven by changes in the lateral transport of water masses supplying oxygen-rich waters to low-oxygen regions and by changes in the upwelling of deep, nutrient-rich waters affecting net primary productivity (NPP) as demonstrated below.

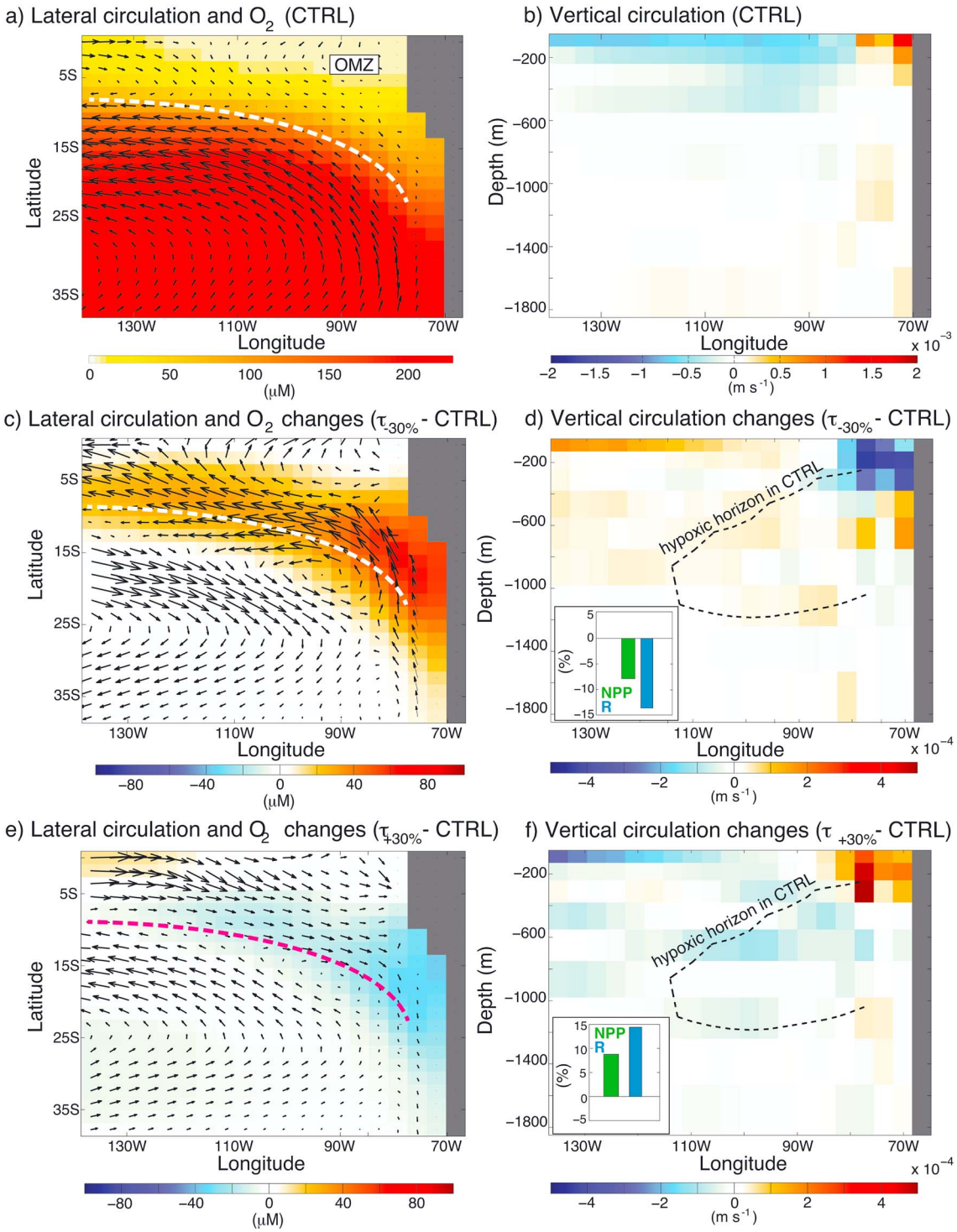


**Figure 9.** (a) Equilibrium oxygen concentration (μM; color shading) and horizontal circulation (m $s^{-1}$; vectors) off Chile in CTRL, both averaged over 240 m to 550 m depth. The dashed line refers to the transition between the westward flowing South Equatorial Current (SEC) and the eastward flowing Equatorial Undercurrent (EUC) System in CTRL. (b) Vertical velocity (m $s^{-1}$) averaged over 0° to 32°S in the Pacific Ocean. (c) As Figure 9a but for $\tau_{-30\%}$ − CTRL. (d) As Figure 9b but for $\tau_{-30\%}$ − CTRL; dashed contour indicates the horizon of the hypoxic volume at 13.5°S in CTRL, which marks the latitude of highest $O_2$ change in this region between $\tau_{-30\%}$ and CTRL. The bar diagram embedded in the figure shows the relative change in net primary productivity (NPP; green bars) and remineralization (R; blue bars) integrated in the water column between 0° and 32°S and 130°W and 70°W ($\tau_{-30\%}$ − CTRL). (e) and (f) As Figures 9a and 9c and Figures 9b and 9d, respectively, but for $\tau_{+30\%}$ − CTRL.

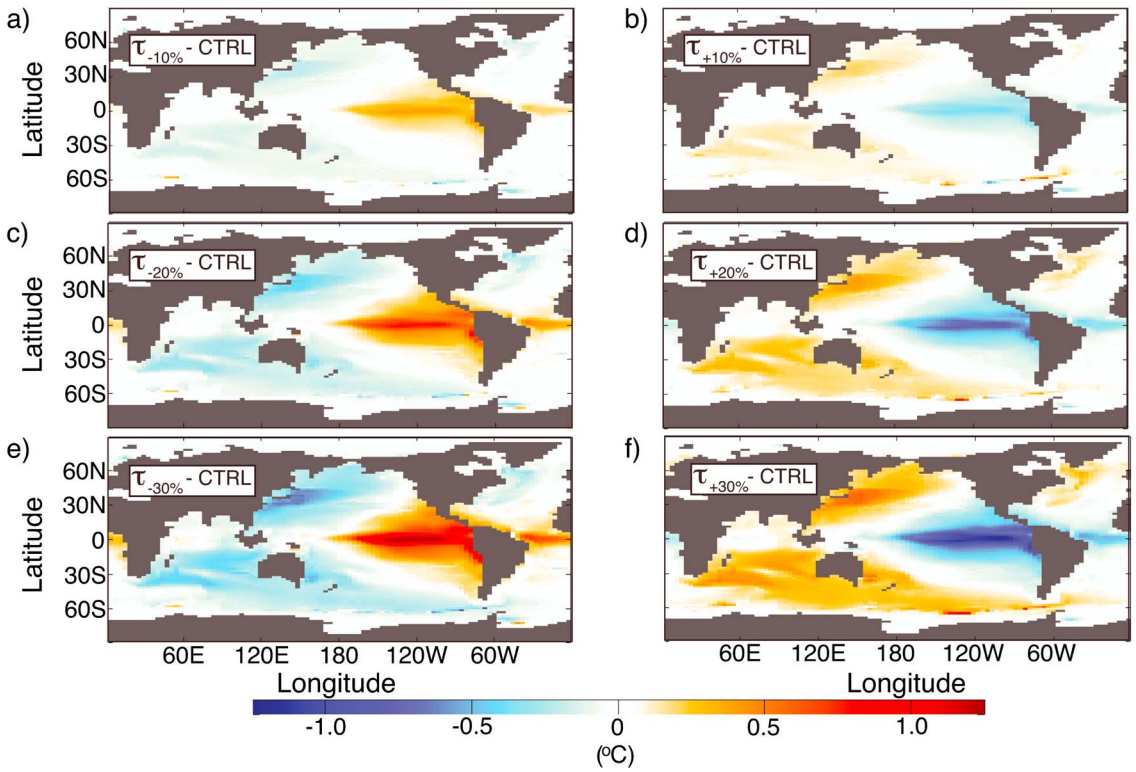


**Figure 10.** Sea surface temperature changes (°C) in all equilibrated perturbation experiments shown relative to CTRL.

Changes in $O_2$ with the oxygen saturation effect removed (Figures 7a and 7b, color) mostly coincide with changes in water age (Figures 7a and 7b, contoured) with younger waters exhibiting higher concentrations. The zero line of both property anomalies coincide in many regions, which shows that as the age and ventilation rate change, so does the oxygen content. This is consistent with *Gnanadesikan et al.* [2012] who found similar results in the Pacific Ocean for their experiments using the Special Report on Emissions Scenarios A2 increasing $CO_2$ emissions scenario.

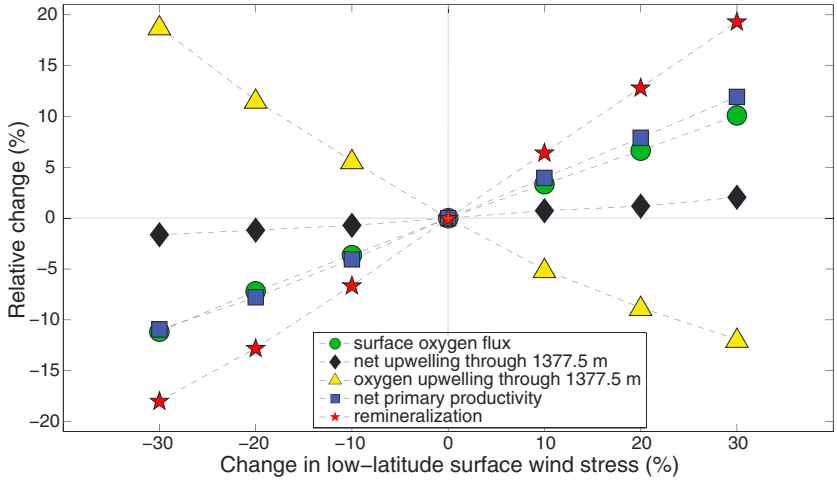


**Figure 11.** Relative changes in various properties area-averaged over the Pacific Ocean between 40°S and 40°N for all wind perturbation experiments relative to control. Shown are the air-sea oxygen flux at the surface (green circles), net upwelling through 1377.5 m (black diamonds; integral of vertical velocity over the 1377.5 m surface), oxygen upwelling through 1377.5 m (yellow triangles; integral of the product between vertical velocity and oxygen concentrations over the 1377.5 m surface), net primary productivity (blue squares), and remineralization (red stars).

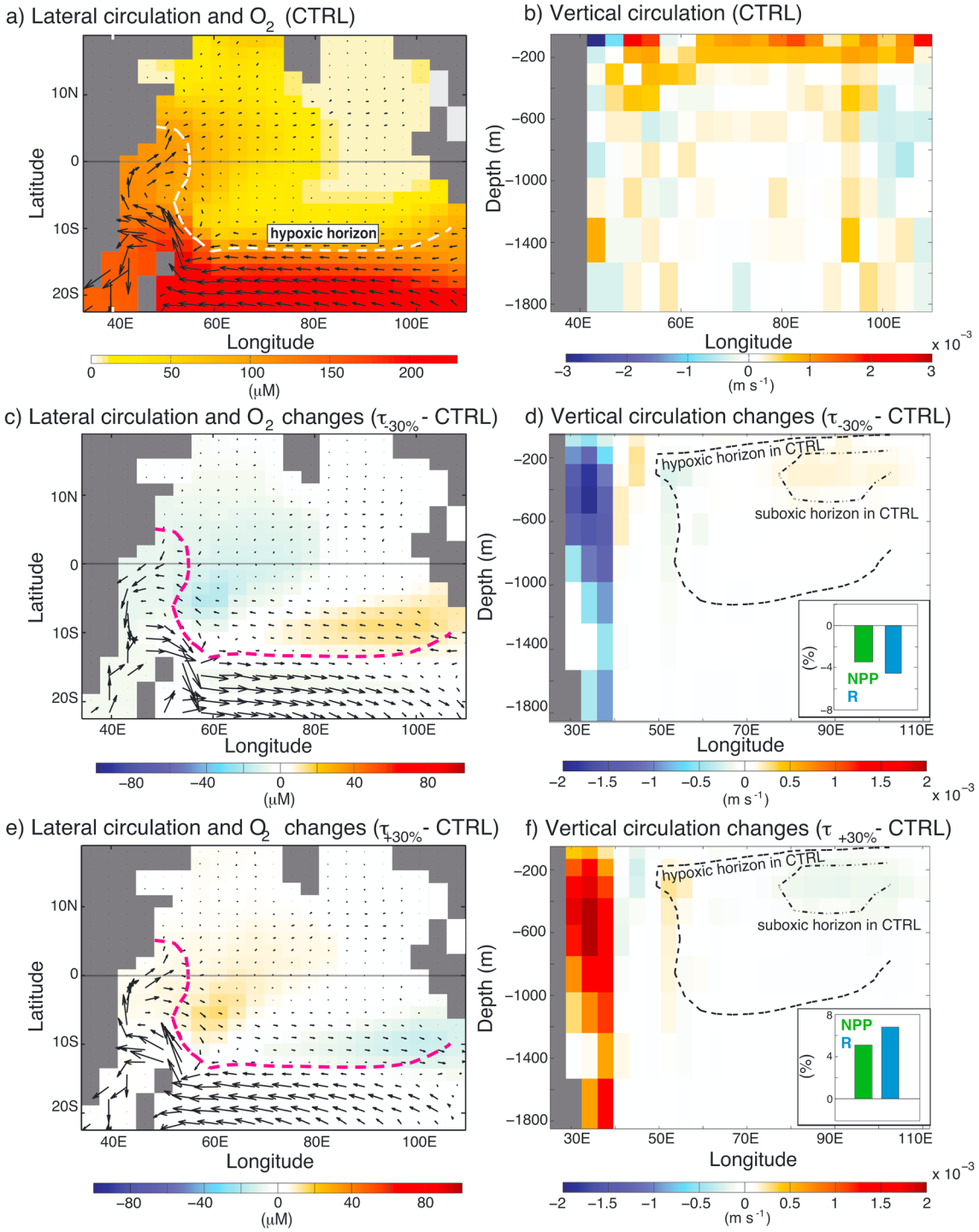


**Figure 12.** (a) Equilibrium oxygen concentration (μM; color shading) and horizontal circulation (m $s^{-1}$; vectors) off Somalia in CTRL, both averaged over 240 m to 550 m depth. (b) Vertical velocity (m $s^{-1}$) averaged over 9.9°N to 9.9°S in the Indian Ocean. (c) As (a) but for $\tau_{-30\%}$ − CTRL. Dashed line represents the 88 μM isoline of $O_2$ averaged between 240 m to 550 m depth in CTRL. (d) As Figure 12b but for $\tau_{-30\%}$ − CTRL; dashed (dashed-dotted) contour indicates the horizon of the hypoxic (suboxic) volume at 4.5°S in CTRL, which marks the latitude of highest $O_2$ change in this region between $\tau_{-30\%}$ and CTRL. The bar diagram embedded in the figure shows the relative change in net primary productivity (NPP, green bars) and remineralization (R, blue bars) integrated in the water column between 9.9°N and 9.9°S and 40°E and 110°E ($\tau_{-30\%}$ − CTRL). (e and f) As Figures 12a and 12c and Figures 12b and 12d, respectively, but for $\tau_{+30\%}$ − CTRL.

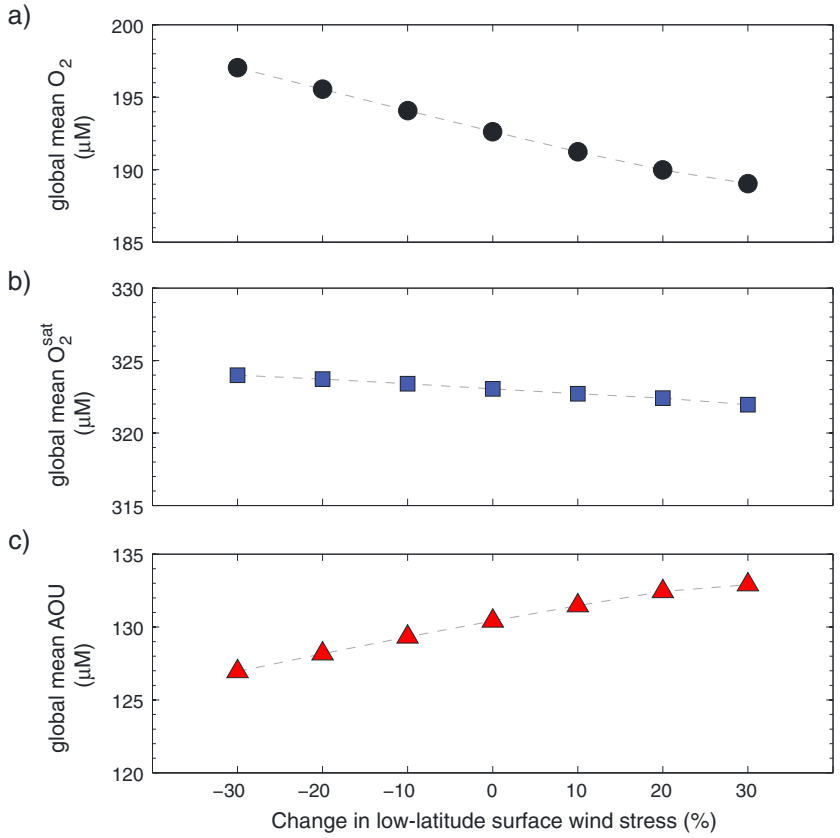


**Figure 13.** Global mean equilibrated (a) oxygen concentration, (b) oxygen saturation concentration ($O_2^{sat}$), and (c) apparent oxygen utilization (AOU) (μM) as a function of low-latitude easterly surface wind stress change (%). The *y* axis scales are offset but each of uniform range.

This correlation between $O_2$ and water age can also be seen in the relationship between changes in $O_2$ concentration and those in age of the corresponding waters for experiments $\tau_{-30\%}$ and $\tau_{+30\%}$ (Figures 7c and 7d). Both experiments exhibit the expected response of $O_2$ concentrations to ventilation and thus water age changes, i.e., higher $O_2$ concentrations in more rapidly ventilated younger waters and vice versa for older waters. However, both experiments also contain waters that contradict the negative correlation between $O_2$ anomalies and age changes. This is especially obvious when looking at the global mean changes in $O_2$ versus age depending on model layer depth (Figure 15). In experiment $\tau_{+30\%}$ (triangles), increased winds lead to

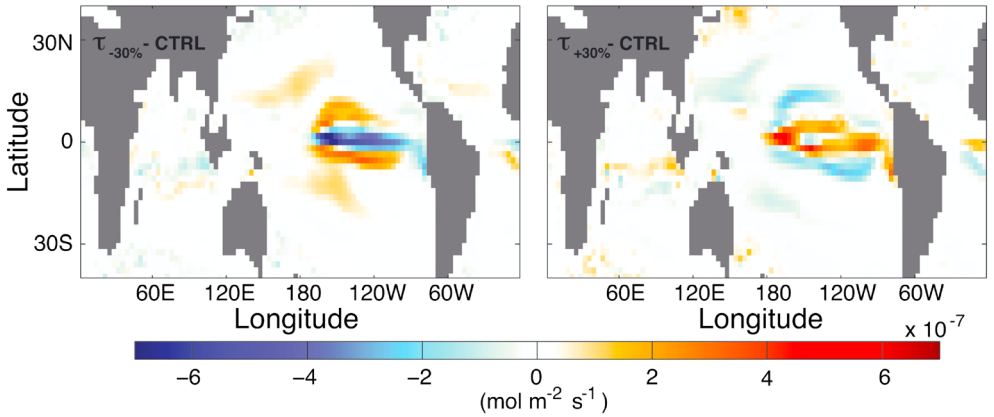


**Figure 14.** Changes in tropical downward air-sea oxygen flux ($10^{-7}$ mol $m^{-2}$ $s^{-1}$) in the equilibrated perturbation experiments (left) $\tau_{-30\%}$ − CTRL and (right) $\tau_{+30\%}$ − CTRL. All experiments in this figure use the corrected stoichiometry ratio between nitrogen and oxygen.

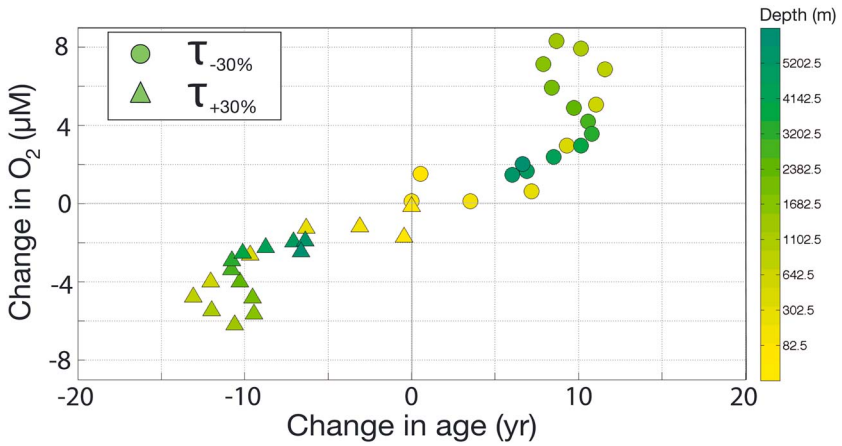


**Figure 15.** Scatterplot of equilibrated mean $O_2$ change (μM) and age change (yr) at different model layers. Dots mark changes in $\tau_{-30\%}$; triangles mark changes in $\tau_{+30\%}$. Colors indicate the model layer from yellow (shallow) to green (deep). Note the uneven depth scale of the model layers.

a more rapid ventilation resulting in younger waters compared to CTRL, especially at greater depth (colors). However, the mean $O_2$ concentration changes in all depth layers indicates a decrease despite the increase in ventilation. Experiment $\tau_{-30\%}$ (circles) shows equivalent results but of opposite sign. This behavior of $O_2$ concentrations in both experiments is counterintuitive to the assumption of increasing oxygenation for increasing ventilation. This indicates that changes in the biological cycling of oxygen, in particular in the remineralization of organic matter, must play a role in the projected changes in $O_2$. These changes are caused by modifications in the net upwelling of nutrients and $O_2$ into the upper ocean (Figure 11). The net upwelling through the 1377.5 m surface for instance changes with the same sign as the applied perturbation (see black diamonds in Figure 11). Consequently experiments $\tau_{-10\%}$, $\tau_{-20\%}$, and $\tau_{-30\%}$ exhibit a reduction in the upwelling of nutrients while the trade wind increase experiments show enhanced upwelling. Accordingly, mean NPP and with this mean export production (not shown) and remineralization rate (R) decrease with weaker equatorial winds and increase when the winds are strengthened (blue squares and red stars in Figure 11, respectively). At greater depths, the reduction in $O_2$ due to decreased NPP under weaker $\tau_x$ is completely compensated for by the decreased use of $O_2$ for remineralization due to a reduced presence of organic matter (see red stars in Figure 11), which in turn results in a higher upwelling of $O_2$ from greater depth, completely compensating the reduced $O_2$ production (see yellow triangles in Figure 11). This is

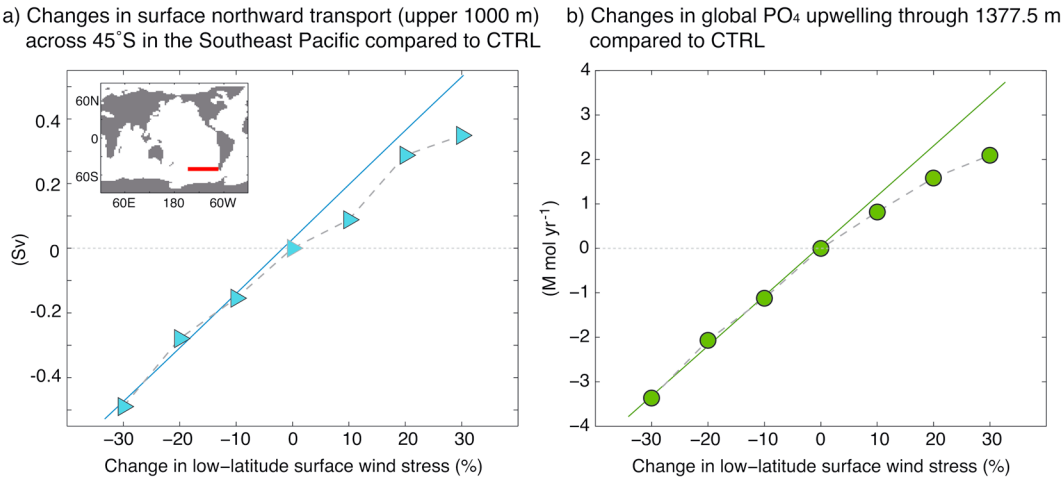


**Figure 16.** (a) Changes in surface northward transport (upper 1000 m) across 45°S in the eastern South Pacific Ocean between 153°W and 70°W (red line) compared to CTRL. Surface northward transport in CTRL is 0.094 Sv. Blue line is the linear fit to the changes in the three reduced wind stress experiments. (b) Changes in global upwelling of $PO_4$ across 1377.5 m depth compared to CTRL (70.44 M mol $PO_4$ $yr^{-1}$). Green line is the linear fit to the changes in the three reduced wind stress experiments.

consistent with the findings of *Matear et al.* [2000] who also found increased $O_2$ concentrations in their model experiments with lower NPP. Under strengthened $\tau_x$ conditions, higher NPP provide more organic matter that is in turn remineralized at depth, leading to lower oxygen concentrations in these experiments. However, the amount of change caused by increased winds is smaller than in the equivalent decreased winds experiment (compare, e.g., Figures 5a and 5b to Figures 7a and 7b). This higher sensitivity to decreased winds is caused by differences in both (i) the northward transport into the southeast Pacific (i.e., ocean transport/ventilation) and (ii) the upwelling of $PO_4$ across intermediate depths resulting from biological processes (Figure 16). For weakened winds the surface northward transport in the upper 1000 m across 45°S between 150°W and 70°W (which catches the eastern limb of the subtropical gyre) decreases (Figure 16a) due to the wind-driven weakening of the subtropical gyre and the equatorial overturning cells [*Ridder et al.*, 2013]. The same mechanism would cause an equivalent increase for stronger winds if the applied wind perturbations were acting in isolation of interior buoyancy changes. However, a decline in the density gradient between high and low latitudes under increased wind conditions dampens the acceleration of the northward transport. This ultimately leads to a nonlinear response in the ventilation of the Pacific Ocean despite the linear increase in forcing of the applied wind perturbations (Figure 16a). The stronger sensitivity in the upwelling of $PO_4$ to weakened winds is caused by variations in wind-driven upwelling in combination with changed deep ocean remineralization. As described above, reduced biological activity for weakened winds decreases remineralization (Figure 11) and thus the formation of $PO_4$ in the deep ocean. Consequently, the $PO_4$ concentration in the upwelled water, whose amount is already reduced due to the weakened equatorial upwelling cells, is reduced. This affects the growth and productivity of phytoplankton, in particular diazotrophs, which are not limited by other nutrients, and thus ultimately the availability of organic material for remineralization. This feedback is limited for strengthened $\tau_x$ through the model's application of a maximum growth rate for diazotrophs. This results in a higher decrease of $PO_4$ upwelling in experiments with weakened winds compared to the equivalent changes in experiments with strengthened winds (Figure 16c).

## 5. Summary and Conclusions

This study demonstrates that the net volume-integrated global ocean oxygen content is inversely proportional to changes in low-latitude surface wind stress. One third of the changes in the global mean $O_2$ concentration is driven by changes in SST and thus $O_2^{sat}$. The remaining two thirds are caused by changes in ocean circulation/ventilation in combination with changes in biological activity. Considering that some waters are more gradually ventilated under decreased wind conditions yet show higher $O_2$ concentrations compared to CTRL (and vice versa for increased $\tau_x$ conditions), changes in marine biological cycling must fundamentally control the response in $O_2$ in addition to ventilation/circulation in these waters. In particular, biological activity responds to the wind-driven changes in upwelling of nutrients, causing a decrease (increase) in NPP for decreased (increased) winds, which then leads to changes in export production and remineralization of the same sign. Put simply, reduced equatorial trade winds lead to decreased biological activity and eventually, over time, to decreased $O_2$ consumption, resulting in increased $O_2$ concentrations in the absence of other changes. This also affects the global low-oxygen volumes which become more oxygenated in experiments with weaker $\tau_x$ and vice versa for strengthened $\tau_x$ conditions. The global response is dominated by changes in the Pacific Ocean, which is more sensitive to a decrease than to an increase in $\tau_x$, showing higher absolute anomalies in experiments $\tau_{-10\%}$, $\tau_{-20\%}$, and $\tau_{-30\%}$ than in the experiments with equivalent $\tau_x$ increases.

The OMZ in the Pacific Ocean off Peru-Chile (at 32°S–8°S, 272°E–290°E and 240–550 m depth) experiences the highest change in $O_2$. For weakened $\tau_x$ conditions this area increases its $O_2$ content due to an increase in ventilation from the south (caused by a weakening of the EUC and SEC) and an increased transport of $O_2$ from greater depths in combination with lower remineralization between 240 m and 550 m. The same processes but of opposite sign cause a decrease in $O_2$ concentrations in this region under strengthened $\tau_x$ conditions. The driving mechanism behind these changes are more along-coast wind conditions in experiments with surface wind stress smaller than CTRL, similar to the findings in *Gnanadesikan et al.* [2012] and more off-shore wind conditions in experiments with higher surface wind stress.

A similar mechanism is at play in the tropical Indian Ocean along the eastern boundary; however, the impact on $O_2$ is mostly compensated by changes in the Indonesian throughflow of Pacific Ocean waters with their altered $O_2$ signature. Along the western boundary, low-oxygen regions in the Indian Ocean become more

depleted of $O_2$ due to a decreased subtropical gyre and thus a decreased ventilation of waters off Somalia from the south. The driving mechanism in this area is a change in wind conditions, similar to the driving mechanism in the Pacific but of opposite sign, i.e., anomalous off-shore conditions in experiments with reduced surface wind stress and higher onshore conditions for increased surface winds.

In conclusion, this study shows that in isolation of other changes, the tropical zonal wind fields alter circulation, SST, and biological cycling in such a way to increase net ocean oxygenation of sea water and to contract the global low-oxygen volume under decreased trade winds, and vice versa for increased $\tau_x$. Under reduced wind stress, as is projected to occur during the 21st century [e.g., *Collins et al.*, 2010], the weakened equatorial overturning cells would cause a deceleration of the Ekman transport and thus a reduction in poleward heat transport away from the equator. The resulting colder SST in the subtropics and at middle and high latitudes would then lead to higher oxygen concentrations in waters that are subsequently transported into the ocean interior, ultimately increasing global mean dissolved oxygen. At the same time the supply of nutrients to the photic zone would be decreased due to a weakening in the upwelling branch of the overturning, resulting in overall-reduced NPP and with this oxygen depletion via remineralization. Increased trade winds would lead to the opposite effect of increased nutrient supply to the photic zone and thus higher NPP and remineralization.

**Acknowledgments**
This study was funded by the ARC and supported by an award under the Merit Allocation Scheme on the NCI National Facility at the ANU. We acknowledge the help of Willem Sijp during the set up of the model on the NCI system. The authors thank Niki Gruber for his input at the early stages of this project and Andreas Oschlies for his valuable support and input during the review process, along with an anonymous reviewer, which helped improve this study considerably.

## References

Archer, D. (1996), A data-driven model of the global calcite lysocline, *Global Biogeochem. Cycles*, *10*, 511–526.
Bopp, L., C. Le Quéré, M. Heimann, A. C. Manning, and P. Monfray (2002), Climate-induced oceanic oxygen fluxes: Implications for the contemporary carbon budget, *Global Biogeochem. Cycles*, *16*, 1022, doi:10.1029/2001GB001445.
Clarke, A. J., and A. Lebedev (1996), Long-term changes in the equatorial pacific trade winds, *J. Clim.*, *9*, 1020–1029.
Cline, J. D., and F. A. Richards (1972), Oxygen-deficient conditions nitrate reduction in the eastern tropical North Pacific, *Limnol. Oceanogr.*, *17*, 885–900.
Cocco, V., et al. (2013), Oxygen and indicators of stress for marine life in multi-model global warming projections, *Biogeosciences*, *10*(3), 1849–1868.
Codispoti, L. A., J. A. Brandes, J. P. Christensen, A. H. Devol, S. W. A. Naqvi, H. W. Paerl, and T. Yoshinari (2001), The oceanic fixed nitrogen and nitrous oxide budgets: Moving targets as we enter the anthropocene?, *Sci. Mar.*, *65*, 85–105.
Collins, M., et al. (2010), The impact of global warming on the tropical Pacific Ocean and El Niño, *Nat. Geosci.*, *3*, 391–397.
Duteil, O., and A. Oschlies (2011), Sensitivity of simulated extent and future evolution of marine suboxia to mixing intensity, *Geophys. Res. Lett.*, *38*, L06607, doi:10.1029/2011GL046877.
England, M. H. (1995), The age of water and ventilation timescales in a global ocean model, *J. Phys. Oceanogr.*, *25*, 2756–2777.
England, M. H., S. McGregor, G. A. Meehl, A. Timmermann, W. Cai, A. Sen Gupta, M. J. McPhaden, A. Purich, and A. Santoso (2014), Recent intensification of wind-driven circulation in the Pacific and the ongoing warming hiatus, *Nat. Clim. Change*, *4*, 222–227.
Frölicher, T. L., F. Joos, G.-K. Plattner, M. Steinacher, and S. C. Doney (2009), Natural variability and anthropogenic trends in oceanic oxygen in a coupled carbon cycle-climate model ensemble, *Global Biogeochem. Cycles*, *23*, GB1003, doi:10.1029/2008GB003316.
Gnanadesikan, A., J. P. Dunne, and J. John (2012), Understanding why the volume of suboxic waters does not increase over centuries of global warming in an Earth System Model, *Biogeosciences*, *9*, 1159–1172.
Harrison, D. E. (1989), Post World War II trends in tropical pacific surface trades, *J. Clim.*, *2*, 1561–1562.
Helly, J., and L. Levin (2004), Global distribution of naturally occurring marine hypoxia on continental margins, *Deep Sea Res., Part I*, *51*, 1159–1168.
Hibler, W. D. (1979), A dynamic thermodynamic sea ice model, *J. Phys. Oceanogr.*, *9*, 815–846.
Hunke, E. C., and J. K. Dukowicz (1997), An elastic viscous plastic model for sea ice dynamics, *J. Phys. Oceanogr.*, *27*(9), 1849–1867.
Kalnay, E., et al. (1996), The NCEP/NCAR 40-year reanalysis project, *Bull. Am. Meteorol. Soc.*, *77*, 437–472.
L'Heureux, M. L., S. Lee, and B. Lyon (2013), Recent multidecadal strengthening of the Walker circulation across the tropical Pacific, *Nat. Clim. Change*, *3*, 571–576, doi:10.1038/nclimate1840.
Matear, R. J., and A. C. Hirst (2003), Long-term changes in dissolved oxygen concentrations in the ocean caused by protracted global warming, *Global Biogeochem. Cycles*, *17*, 1125, doi:10.1029/2002GB001997.
Matear, R. J., A. C. Hirst, and B. I. McNeil (2000), Changes in dissolved oxygen in the Southern Ocean with climate change, *Geochem. Geophys. Geosyst.*, *1*, 1050, doi:10.1029/2000GC000086.
Meissner, K. J., A. J. Weaver, H. D. Matthews, and P. M. Cox (2003), The role of land surface dynamics in glacial inception: A study with the UVic Earth System Model, *Clim. Dynam.*, *21*, 515–537.
Oguz, T., H. W. Ducklow, and P. Malanotte-Rizzoli (2000), Modeling distinct vertical biogeochemical structure of the Black Sea: Dynamical coupling of the oxic, suboxic, and anoxic layers, *Global Biogeochem. Cycles*, *14*, 1331–1352.
Oschlies, A., K. G. Schulz, U. Riebesell, and A. Schmittner (2008), Simulated 21st century's increase in oceanic suboxia by $CO_2$-enhanced biotic carbon export, *Global Biogeochem. Cycles*, *22*, GB4008, doi:10.1029/2007GB003147.
Pacanowski, R. C. (1995), MOM 2 documentation: User's guide and reference manual, version 1.0, *GFDL Ocean Group Tech. Rep. 3*, Geophys. Fluid Dyn. Lab., Princeton, N. J.
Paulmier, A., and D. Ruiz-Pino (2009), Oxygen Minimum Zones (OMZs) in the modern ocean, *Prog. Oceanogr.*, *80*, 113–128.
Reid, J. L., Jr. (1965), *Intermediate Waters of the Pacific Ocean*, vol. 2, Johns Hopkins Univ. Press, Baltimore, Md.
Ridder, N. N., K. J. Meissner, and M. H. England (2013), Sensitivity of the oceanic carbon reservoir to tropical surface wind stress variations, *Geophys. Res. Lett.*, *40*, 2218–2223, doi:10.1002/grl.50498.
Rodgers, K. B., B. Blanke, G. Madec, O. Aumont, P. Ciais, and J.-C. Dutay (2003), Extratropical sources of equatorial Pacific upwelling in an OGCM, *Geophys. Res. Lett.*, *30*, 1084, doi:10.1029/2002GL016003.
Sarmiento, J., N. Gruber, M. Brzezinski, and J. Dunne (2004), High-latitude controls of thermocline nutrients and low latitude biological productivity, *Nature*, *427*, 56–60.

Schmittner, A., A. Oschlies, H. D. Matthews, and E. D. Galbraith (2008), Future changes in climate, ocean circulation, ecosystems, and biogeochemical cycling simulated for a business-as-usual $CO_2$ emission scenario until year 4000 AD, *Global Biogeochem. Cycles*, *22*, GB1013, doi:10.1029/2007GB002953.

Semtner, A. J., Jr. (1976), A model for the thermodynamic growth of sea ice in numerical investigations of climate, *J. Phys. Oceanogr.*, *6*, 379–389.

Shaffer, G., S. M. Olsen, and J. O. P. Pedersen (2009), Long-term ocean oxygen depletion in response to carbon dioxide emissions from fossil fuels, *Nat. Geosci.*, *2*, 105–109.

Stramma, L., G. C. Johnson, J. Sprintall, and V. Mohrholz (2008), Expanding oxygen minimum zones in the tropical oceans, *Science*, *320*, 655–658.

Stramma, L., G. C. Johnson, E. Firing, and S. Schmidtko (2010), Eastern Pacific oxygen minimum zones: Supply paths and multidecadal changes, *J. Geophys. Res.*, *115*, C09011, doi:10.1029/2009JC005976.

Stramma, L., A. Oschlies, and S. Schmidtko (2012), Mismatch between observed modeled trends in dissolved upper-ocean oxygen over the last 50 yr, *Biogeosciences*, *9*, 4045–4057.

Tokinaga, H., and S.-P. Xie (2011), Weakening of the equatorial Atlantic cold tongue over the past six decades, *Nat. Geosci.*, *4*(4), 222–226.

Tokinaga, H., S.-P. Xie, A. Timmermann, S. McGregor, T. Ogata, H. Kubota, and Y. M. Okumura (2012), Regional patterns of tropical Indo-Pacific climate change: Evidence of the Walker circulation weakening, *J. Clim.*, *25*, 1689–1710.

Trenberth, K. E., and J. W. Hurrell (1994), Decadal atmosphere-ocean variations in the Pacific, *Clim. Dynam.*, *9*, 303–319.

Vecchi, G. A., and B. J. Soden (2007), Global warming the weakening of the tropical circulation, *J. Clim.*, *20*, 4316–4340.

Vecchi, G. A., B. J. Soden, A. T. Wittenberg, I. M. Held, A. Leetmaa, and M. J. Harrison (2006), Weakening of tropical Pacific atmospheric circulation due to anthropogenic forcing, *Nature*, *441*, 73–76.

Weaver, A., et al. (2001), The UVic Earth System Climate Model: Model description, climatology and application to past, present and future climates, *Atmosphere-Ocean*, *39*, 361–428.

Weiss, R. F. (1970), The solubility of nitrogen, oxygen and argon in water and seawater, *Deep-Sea Res.*, *17*, 721–735.